

Gradient Enhanced Image Pyramid for Improved Nonlinear Image Registration

Lin Gan and Gady Agam,
Illinois Institute of Technology, Chicago, IL, USA

Abstract

In this paper we investigate the use of image pyramid within a hierarchical registration framework for improved nonlinear image registration. Gaussian image pyramid is commonly used to reduce image complexity so that registration can be performed in a coarse to fine manner. In this paper, we apply two edge preserving filters, the bilateral filter and the guided filter, to generate image pyramids that can preserve strong gradient so as to improve registration accuracy. In addition, we propose a bilateral fractional differential based image enhancement filter and combine its output with a guided filter to generate another image pyramid that further enhances the gradient of strong image components. Registration is performed within a hierarchical framework where the model complexity of a Discrete Cosine Transformation (DCT) based nonlinear model is increased to couple with the image pyramid. Different image pyramids are compared by using three types of synthetic deformation fields. Experimental results show that registration using the gradient enhanced image pyramid achieves more accurate registration than registration using the Gaussian image pyramid.

Introduction

Image registration aims to establish one-to-one spatial correspondence between two or more images of a same scene or several similar scenes. It serves as an important pre-processing step to image analysis tasks such as image fusion, change detection and multi-channel image restoration. It is also a fundamental component in a variety of applications including remote sensing, medical imaging, robot vision.

Image registration is an ill-posed problem where a minor change in the input can lead to a totally different solution. Especially for nonlinear image registration, factors such as the similarity metric, deformation model, and optimization method all play important roles. In this paper we keep most of the factors in control so as to investigate the use of image pyramid in a nonlinear image registration context.

Image registration problems are commonly solved hierarchically in a coarse to fine manner. This is done either in the image space or in a transformation space. The purpose of using hierarchical registration is to first match global components at a coarse level and gradually matching the more intricate components at finer levels. The hope is that the reduction of complexity can help avoid local minima traps in the optimization process.

In image space, the reduction of complexity is often achieved by smoothing the input image with increasing amounts. The stack of such increasingly simplified version of the input image is called image scale space [1]. If the smoothed image is also downsampled at each level, the obtained image is not only less complex but

also contains less amount of data. When a Gaussian smoothing filter is applied and the downsampling factor is selected as 2, we obtain the commonly used Gaussian image pyramid.

The Gaussian image pyramid has been widely used in image registration problems, especially in linear registration using rigid or affine transformation models. The reduction of image size in the pyramid is particularly helpful for registration involving large transformations. It is also straightforward to propagate estimations obtained from a coarse level to a finer level in the parameter field for linear registration.

The Gaussian image pyramid has been used in nonlinear registration [2, 3] where it is often applied to 3-D registration problems to reduce the amount of processing at coarse stages. However, a problem of using the Gaussian image pyramid for nonlinear image registration is the propagation of estimations from a coarse level to a finer level. Deformation estimation at a coarse level have to be upsampled to form the initial deformation for the larger images at the next finer level. Such upsampling step can be problematic because artifacts can emerge during the interpolation process. An even more complicated process happens if such upsampled deformation field has to be transformed back into coefficients, such as in basis function based deformation models. Therefore, an alternative of the traditional Gaussian image pyramid is the image scale space where images are only smoothed but not downsampled. In this manner parameters obtained at a coarse level can be directly used as the initial value for parameters at a finer level.

While image complexity is reduced by using the Gaussian image pyramid, the sensitivity to the image gradient is also weakened. Image components such as edges are supposed to provide strong guidance to the registration process. Since all image pixels are uniformly smoothed in the Gaussian smoothing process, gradient at such image components is greatly reduced. Such reduction have more impact for the coarser levels where the smoothing amount is large. The consequence is that registration at coarse levels may fail to provide a good initial estimation which is often difficult to rectify in finer levels.

In this paper, we apply two edge preserving filters, a bilateral filter and a guided filter, to generate two alternative image pyramids to the Gaussian pyramid. The produced image pyramids preserve strong edges better than those at the same level of the Gaussian image pyramid. In addition, we propose a bilateral fractional differential filter to enhance strong edges in the image. The enhanced image is used as a guide image in a guided filter to produce a new image pyramid where the strong edges are enhanced. It should be pointed out that the word pyramid is kept to refer to images at different level, even though they are of the same size but at different smoothing level.

To evaluate the performance of registrations using different image pyramids, we generated three types of synthetic deformations: a radial deformation, a sinusoidal deformation and a random deformation. The synthetic deformations were applied to a pool of images including brain, chest and lung images with various contrast levels. The synthetic deformation field was used as the ground truth and compared to the estimated deformation field. We also computed two other metrics to measure the similarity between the registered image and the target image, and the regularity of the estimated deformation field. Experimental results show that using gradient enhanced image pyramid improves the registration by having a smaller mean deformation field error.

Methods

In this section we first present two edge preserving filters: the bilateral smoothing filter and the guided smoothing filter. Then a fractional differential based enhancement filter is introduced where its output is applied in the guided filter as the guide image.

Image Pyramid using Bilateral Filter

The bilateral filter is a nonlinear filter originally proposed by Tomasi and Manduchi in [4]. It has strong connection with the Gaussian filter. The Gaussian filter is defined as:

$$\hat{I}(x) = \frac{1}{W_1} \sum_{x_i \in \Omega} g_s(\|x - x_i\|) I(x_i) \quad (1)$$

where $I(x)$ and $\hat{I}(x)$ are the input image and the filtered image, Ω is a spatial neighborhood centered at x , and W_1 is a normalization factor such that:

$$W_1 = \sum_{x_i \in \Omega} g_s(\|x - x_i\|) \quad (2)$$

where $g_s(\|x - x_i\|)$ is a Gaussian function such that:

$$g_s(\|x - x_i\|) = e^{-\frac{(x-x_i)^2}{2s^2}} \quad (3)$$

The smoothing weight of each pixels x_i within Ω is determined by its distance from x and the Gaussian standard deviation s . This Gaussian function is commonly referred to as the spatial filter.

The bilateral filter is defined as:

$$\hat{I}(x) = \frac{1}{W_2} \sum_{x_i \in \Omega} g_s(\|x - x_i\|) h_r(\|I(x) - I(x_i)\|) I(x_i) \quad (4)$$

where an additional weight function $h_r(\|I(x) - I(x_i)\|)$ is included which is also a Gaussian function such that:

$$h_r(\|I(x) - I(x_i)\|) = e^{-\frac{(I(x)-I(x_i))^2}{2r^2}} \quad (5)$$

where r is the standard deviation of the Gaussian function that controls the fall off of the weight in the intensity domain. It is commonly referred to as the range filter.

Similarly, W_2 is a normalization factor such that:

$$W_2 = \sum_{x_i \in \Omega} g_s(\|x - x_i\|) h_r(\|I(x) - I(x_i)\|) \quad (6)$$

The smoothing weight of a pixel x_i is now decided by both the spatial distance from x and its intensity difference from x . As can be observed, higher weight is given to pixels that are both spatially close to x and similar to x in intensity. By combining the spatial filter and the range filter, strong smoothing is performed in low variance regions while less strong smoothing is performed in high variance regions thus preserving edges. The bilateral filter has been widely used in image denoising [5], edge detection [6], and image enhancement [7]. The limitation of the bilateral filter is that it is slow when the kernel size is large. In addition, the filter can produce stair-case effect [8] which may be undesired in some applications. Moreover, it has been shown in [9] that the gradient at edge pixels in the filter image can be reversed.

We use the bilateral smoothing kernel to replace the Gaussian smoothing kernel in producing the image pyramid. The size of the kernel window is increased for coarse levels. Strong image features such as edges are expected to be less smoothed thus enhancing the gradient at those pixels. Such enhanced gradient is expected to better guide the registration process.

Image Pyramid using Guided Filter

As another edge preserving filter, the guided smoothing filter was proposed in [10]. The guided filter uses an additional guidance image and its output is a locally linear transformation of the guidance image and the input image. It is defined as:

$$\hat{I}_i = a_k G_i + b_k, \forall i \in \Omega_k \quad (7)$$

where G is the guidance image and \hat{I} is the filtered image. Ω_k is a square window centered at pixel k , and a_k and b_k are the linear coefficients that are constants in Ω_k . Since $\nabla \hat{I} = a \nabla G$, the linear model ensures that \hat{I} has an edge only if G has an edge. The local constant a_k and b_k are solved by minimizing a cost function in window Ω_k between the filtered image and the input image I , such that:

$$\begin{aligned} E(a_k, b_k) &= \sum_{i \in \Omega_k} \left((\hat{I}_i - I_i)^2 + \varepsilon a_k^2 \right) \\ &= \sum_{i \in \Omega_k} \left((a_k G_i + b_k - I_i)^2 + \varepsilon a_k^2 \right) \end{aligned} \quad (8)$$

where ε is a regularization factor to prevent large a_k . By using linear ridge regression, the solution is given by:

$$a_k = \frac{\frac{1}{|\Omega_k|} \sum_{i \in \Omega_k} (G_i I_i - \mu_k \bar{I}_k)}{\sigma_k^2 + \varepsilon} \quad (9)$$

$$b_k = \bar{I}_k - a_k \mu_k \quad (10)$$

where μ_k and σ_k^2 are the mean and variance of G in window Ω_k , $|\Omega_k|$ is the number of pixels in window Ω_k , and $\bar{I}_k = \frac{1}{|\Omega_k|} \sum_{i \in \Omega_k} I_i$ is the mean of I in window Ω_k .

Since windows can be placed at all pixels, we will have the same number of windows as pixels in the image. Accordingly, the filtered value of each pixel is also affected by $|\Omega_k|$ windows. In [10] the computed a_k and b_k values in all windows affecting a pixel are averaged such that:

$$\begin{aligned} \hat{I}_i &= \frac{1}{|\Omega_i|} \sum_{k: i \in \Omega_k} (a_k G_i + b_k) \\ &= \bar{a}_i G_i + \bar{b}_i \end{aligned} \quad (11)$$

where $\bar{a}_i = \frac{1}{|\Omega_i|} \sum_{k \in \Omega_i} (a_k)$ and $\bar{b}_i = \frac{1}{|\Omega_i|} \sum_{k \in \Omega_i} (b_k)$, and $|\Omega_i| = |\Omega_k|$ are the number of windows affecting a pixel i .

The guide image G can be the same as the input image I . If they are the same (9) and (10) are converted to $a_k = \frac{\sigma_k^2}{\sigma_k^2 + \varepsilon}$ and $b_k = (1 - a_k) \mu_k$. It can be seen that a_k approaches 1 and b_k approaches 0 when the variance is high in a window. In such a case the filtered image takes more of the input image thus reducing the smoothing effect and preserving high variance features. On the other hand, a_k approaches 0 and b_k approaches 1 when the variance in the window is smaller than a threshold ε . This indicates that the filtered image takes more of the image mean for low variance regions thus achieving smoothing.

Box kernel was used in the original guided filter [10] to compute the image mean, as well as to average the values of a_k and b_k in all windows. Since we use the guided filter to replace the Gaussian filter to produce the image pyramid for registration, we replace the box kernel with a Gaussian kernel in the guided filter so that the filtered image demonstrates similar properties to the Gaussian smoothed image at low variance regions. At high variance regions strong image features are preserved thus enhancing the gradient of strong image features. We use the same input image as the guidance image when performing the guided filtering.

Image Pyramid based on enhanced Guided Filter

In order to further enhance the gradient at strong image features, we apply image enhancement through the use of a fractional differential based filtering. The enhanced image is then used as the guidance image in the guided filter.

Integral differential operators such as Sobel and Laplacian of Gaussian have been widely used for enhancing high frequency features. Such operators have also been extended to non integer cases to form the fractional differential operators. Fractional differential operators have the advantage of being able to enhance image details at low frequency regions. Such operators have been used for edge detection [11], texture enhancement [12], and faint object detection [13].

We use the Grunwald Letnikov fractional differential definition such that:

$$D^\alpha f(x) = \lim_{h \rightarrow 0} \frac{1}{h^\alpha} \sum_{m=0}^{\frac{x-a}{h}} \frac{(-1)^m \Gamma(\alpha+1)}{m! \Gamma(\alpha-m+1)} f(x-mh) \quad (12)$$

where α is the fractional order, h is the differential step, $\Gamma(\cdot)$ is the Gamma function such that $\Gamma(\alpha+1) = \alpha\Gamma(\alpha) = \alpha!$. The first few terms of this fractional operator are computed as $1, -\alpha, \frac{-\alpha(-\alpha+1)}{2}, \frac{-\alpha(-\alpha+1)(-\alpha+1)}{2}, \dots$.

In this paper we give an image kernel by mapping the expanded terms of (12) to coefficients starting from the center. For example, a 5×5 fractional enhancement kernel is constructed as follows:

$$K = \frac{1}{W_3} \begin{bmatrix} b_1 & b_2 & b_3 & b_4 & b_5 \\ b_{16} & a_1 & a_2 & a_3 & b_6 \\ b_{15} & a_8 & 1 & a_4 & b_7 \\ b_{14} & a_7 & a_6 & a_5 & b_8 \\ b_{13} & b_{12} & b_{11} & b_{10} & b_9 \end{bmatrix} \quad (13)$$

where $\sum a_i = -\alpha$, $\sum b_i = \frac{-\alpha(-\alpha+1)}{2}$ and W_3 is a normalization factor to ensure the sum of the kernel is equal to 1. In addition, we

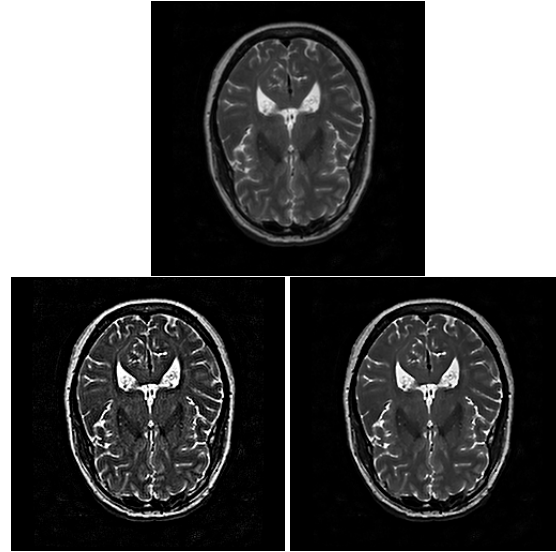


Figure 1. Image enhancement using the fractional differential filter with and without the range filter. Top: original image; bottom left: enhancement without range filter; bottom right: enhancement with range filter, range filter standard deviation $u = 10$.

normalize each coefficient that is not at the kernel center by $\frac{\sum d_i}{d_i}$, where d_i is the Euclidean distance between the coefficient and the kernel center, and $\sum d_i$ is the sum of the Euclidean distance of all the coefficients on the same layer deviated from the kernel center.

We follow the concept of the bilateral smoothing filter and add an additional Gaussian based range filter to the enhancement kernel to produce a bilateral fractional enhancement filter. The range filter is defined by:

$$s_u(\|I(x) - I(x_i)\|) = 1 - e^{-\frac{(I(x) - I(x_i))^2}{2u^2}} \quad (14)$$

where u is the standard deviation of the Gaussian function. The combined bilateral enhancement kernel performs strong fractional differential operation on pixels that are largely different from the center pixel in intensity. Since we use the filtered image as the guidance image in the guided filter, we only want to enhance the most important features but not the details in low variance regions. Figure 1 shows an example of enhancing a 2-D brain image using the fractional differential kernel without and with the range filter. The fractional differential order is $\alpha = 0.5$ and the range filter standard deviation is $u = 10$. It can be seen that by including the range filter, the produced bilateral enhancement filter avoids enhancing image details at low variance regions.

When applying the enhanced image to the guided filter for generating an image pyramid, we vary the standard deviation u of the range filter. A large u is used for smoothing an image for the coarse level so that only the most important image components get enhanced. u is reduced for finer levels where more details can be enhanced.

Implementation Details

In the following section we refer the source image as f and the target image as g .

Nonlinear Deformation Model

We use the DCT basis functions to model the displacement field in the nonlinear registration [14]. DCT has been widely used in image processing due to its near optimal performance in coding for compression. When used in image registration, a displacement field can be represented by a linear combination of the DCT basis functions. A small number of basis functions at low frequencies are sufficient to achieve a satisfactory approximation of the deformation field.

Using inverse mapping, the displacement from a pixel $\mathbf{x} = (x, y)$ in g to a corresponding pixel $\mathbf{x}' = (x', y')$ in f can be represented by:

$$\begin{cases} x' = x - \sum_{j=1}^J (t_j^x B_j(\mathbf{x})) \\ y' = y - \sum_{j=1}^J (t_j^y B_j(\mathbf{x})) \end{cases} \quad (15)$$

where J is the total number of DCT coefficients in 2-D, and $B_j(\mathbf{x})$ is the j -th 2-D DCT basis function at pixel \mathbf{x} . The superscript of t_j denotes the corresponding dimension.

The 2-D DCT basis function can be computed from the separable 1-D DCT basis functions: $b_{j_x}^x(x)$ in the x direction and $b_{j_y}^y(y)$ in the y direction, such that:

$$B_j(\mathbf{x}) \equiv b_{j_x}^x(x) b_{j_y}^y(y) \quad (16)$$

where the subscript $j = j_y J_x + j_x$ with J_x and J_y being the number of coefficients of the preserved 1-D DCT basis functions in the x and y directions respectively.

The k -th 1-D DCT basis function at position l is defined as:

$$b_k(l) = \sqrt{\frac{2}{L}} w(l) \cos\left(\frac{(2l+1)\pi k}{2L}\right) \quad (17)$$

$$w(l) = \begin{cases} \sqrt{\frac{1}{2}} & \text{if } l \equiv 0 \\ 1 & \text{otherwise} \end{cases} \quad (18)$$

where $l \in [0, L)$, and L is the function length in 1-D.

The parameter of the nonlinear deformation model is thus defined as a $2J \times 1$ vector \mathbf{t} with \mathbf{t}^x and \mathbf{t}^y being the column vectors containing the coefficients of the stacked rows of 2-D basis functions in the x and y directions respectively:

$$\mathbf{t} \equiv [(\mathbf{t}^x)^T, (\mathbf{t}^y)^T]^T \quad (19)$$

Optimization Solution

By using the Sum of Squared Difference (SSD) as the similarity metric, the error function is defined as:

$$E(\mathbf{t}) = \sum e(\mathbf{x})^2 = \sum (f(T(\mathbf{x})) - g(\mathbf{x}))^2 \quad (20)$$

where $T(\mathbf{x})$ is the estimated deformation at \mathbf{x} .

In order to enforce smoothness of the estimated deformation field, we add a regularization term that is based on the bending energy of the deformation field, which is defined by:

$$R(\mathbf{t}) = \sum_{\mathbf{x}} \left(\left(\frac{\partial^2 T(\mathbf{x})}{\partial x^2} \right)^2 + \left(\frac{\partial^2 T(\mathbf{x})}{\partial y^2} \right)^2 + 2 \left(\frac{\partial^2 T(\mathbf{x})}{\partial x \partial y} \right)^2 \right)$$

Given the basis function based representation in (15), the bending energy term can be efficiently computed by:

$$R(\mathbf{t}) = \mathbf{t}^T \mathbf{H} \mathbf{t} \quad (22)$$

where \mathbf{H} has the format of:

$$\begin{bmatrix} \bar{\mathbf{H}} & 0 \\ 0 & \bar{\mathbf{H}} \end{bmatrix}$$

for the 2-D case. Matrix $\bar{\mathbf{H}}$ can be pre-computed by:

$$\begin{aligned} \bar{\mathbf{H}} = & (\mathbf{B}_2''^T \mathbf{B}_2'') \otimes (\mathbf{B}_1^T \mathbf{B}_1) + (\mathbf{B}_2^T \mathbf{B}_2) \otimes (\mathbf{B}_1''^T \mathbf{B}_1'') \\ & + 2 (\mathbf{B}_2'^T \mathbf{B}_2') \otimes (\mathbf{B}_1^T \mathbf{B}_1) \end{aligned} \quad (23)$$

where \mathbf{B}_1 and \mathbf{B}_2 are the transformation matrices whose components can be pre-computed based on (16). And \mathbf{B}_1' , \mathbf{B}_1'' , \mathbf{B}_2' and \mathbf{B}_2'' are the transformation matrices involving the first and the second order derivatives of \mathbf{B}_1 and \mathbf{B}_2 , they can also be computed based on (16).

Combine (20) and (22), we can derive a Gauss-Newton based iterative solution such that:

$$\Delta \mathbf{t} = -(\mathbf{A}^T \mathbf{A} + \lambda \mathbf{H})^{-1} (\mathbf{A}^T \mathbf{e} + \lambda \mathbf{H} \mathbf{t}) \quad (24)$$

where \mathbf{e} is the stacked image error vector at all pixels, \mathbf{A} is the Jacobian matrix of image error \mathbf{e} with respect to parameter vector, and λ is a factor to control the regularization weight.

Multi-stage Registration

In order to improve the registration performance, we perform a two-stage image registration process. First, f is translated to match the center of mass to that of the target image g . Then a global affine registration is performed within a multi-resolution framework. The Gaussian image pyramid is used at this stage to account for possible large deformations. Affine parameters are propagated between pyramid levels by scaling up the translation components.

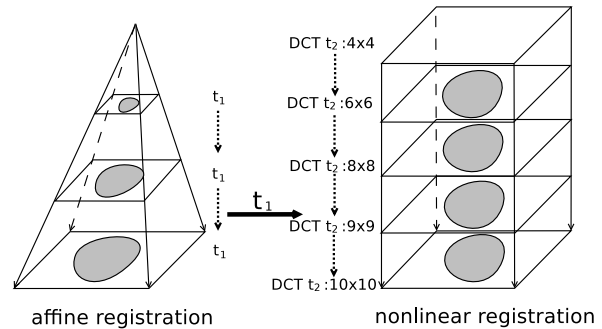


Figure 2. Two stage image registration framework.

Second, a global nonlinear registration using the DCT basis function model is used to perform the multi-level nonlinear image registration. Different image pyramids are constructed and

evaluated at this stage. Figure 2 shows the adopted registration framework. Specifically, we construct a 5 level image pyramid. It can be seen that images in the image pyramid at the nonlinear registration stage are not downsampled. The model parameter is increased along the image pyramid so that simpler model is first used for registration at the coarse levels, the number of parameters is increased for the model at the finer levels.

Evaluation

Evaluation Design

We compared 4 image pyramids: the Gaussian image pyramid, the bilateral image pyramid, the guided image pyramid using the original image as the guidance image, and the guided image pyramid where the fractional differential enhanced image is used as the guidance image.

To evaluate the performance of each registration, we generate three types of synthetic deformations. The first synthetic deformation used a sinusoidal function, which is defined as:

$$\begin{cases} x' = x - \tau_x \sin\left(\frac{y\pi}{\phi_x}\right) \\ y' = y - \tau_y \sin\left(\frac{x\pi}{\phi_y}\right) \end{cases} \quad (25)$$

where (x, y) is the coordinate of the source pixel and (x', y') is that of deformed pixel, τ_x and τ_y control the magnitude of the deformation, ϕ_x and ϕ_y are the phases of the sinusoidal function in the x and y directions respectively.

The second synthetic deformation used a forward radial deformation function, which is defined as:

$$\begin{cases} x' = x + \tau_x (x - r_x) e^{-\frac{(x-r_x)^2 + (y-r_y)^2}{2\sigma^2}} \\ y' = y + \tau_y (y - r_y) e^{-\frac{(x-r_x)^2 + (y-r_y)^2}{2\sigma^2}} \end{cases} \quad (26)$$

where τ_x and τ_y define the magnitude of the deformation, (r_x, r_y) is the center of the radial deformation, σ controls the expansion of the Gaussian function. Using forward radial deformation can lead to a hole in an area around the radial center. Therefore, instead of computing a forward deformation for every pixels in the image, only a number of control points on a regular grid were selected. These corresponding control point pairs were used to interpolate a full deformation field using the thin plate spline [15].

For the third synthetic deformation we generated random displacement for a number of control points on a regular grid. Deformations for all pixels were then interpolated using the thin plate spline. The random displacements were generated using different normal distributions.

The generated synthetic deformations were applied to a pool of images to generate corresponding warped images. Then, the input and warped image pairs were used as source and target images, respectively. The image pool was composed of 2-D slices extracted from 3-D brain images, and chest and lung images. We selected 40 3-D brain images randomly from a public database [16] including 10 T1 images, 10 T2 images, 10 proton density (PD) weighted images and 10 magnetic resonance angiography (MRA) images. In addition, we selected 40 chest images and 40 lung images from a lung image database [17] with variations in illuminations. Such variation in image sources allowed the testing images to have variable geometric structure and illumination. All

images were resized to 256×256 and the spacing between pixels were set to be 1 pixel. Each of the three types synthetic deformations was applied to each of the images. This gave us a total of 360 image pairs for the experimental evaluation.

Using the synthetic deformation, we computed the rooted mean squared deformation field error (RMDE) between the recovered deformation field and the known one. In addition, we measured the similarity between the resulting warped image and the target image in terms of rooted mean squared image error (RMIE). Lastly, the smoothness of the estimated deformation field was also compared by measuring the ratio of pixels with non-positive Jacobian determinant (RNJD). We gave preference to smoothed deformation field in solutions.

Note that the brain and the chest images in the image pool contain large portions of background region where deformation estimation can be unconstrained. We used a simple segmentation approach to generate masks for all the images in the image pool where an intensity threshold was determined to be 25% of the mean image intensity. Evaluation metrics were computed only in the masked regions.

Results

Table 1 shows the mean and standard deviation of the three evaluation metrics for registrations using the selected 4 image pyramids. As can be observed registration using the bilateral image pyramid produced the smallest mean deformation field error. Further, registration using gradient enhanced image pyramids produced smaller deformation field error than registration using the Gaussian pyramid. When using the original image as the guidance image, registration with image pyramid generated from such guided filter produced the smallest mean image difference. While the fractional enhanced guided image pyramid had the largest mean image error, the deformation field produced by it had the fewest pixels with non-positive Jacobian determinant. It can be seen that registration using the gradient enhanced image pyramid showed improved performance over the commonly used Gaussian image pyramid.

Figure 3 shows the images generated at all pyramid levels for one synthetic deformation case using different image pyramids. Figure 4 shows the corresponding deformation field error (encoded in RGB color) between the estimated deformation field and the known one after registration at each pyramid level. From figure 3 it can be seen that strong image features such as the contours of the brain were better preserved for pyramids other than the Gaussian image pyramid. Such difference is especially clear at the coarsest level (level 5). As a result, the known deformation was more closely recovered by registration using the gradient enhanced image pyramid at that level. For the Gaussian image pyramid, the large estimation error happened at the coarsest level can not be rectified at finer levels.

Conclusion

In this paper we investigate alternative image pyramids to the traditional Gaussian pyramid for hierarchical nonlinear image registration context. By taking advantages of edge preserving filters image pyramid can be produced to better preserve the strong gradient information so that image registration can be better guided. Three types of gradient enhanced image pyramids are compared to the Gaussian pyramid using synthetic deformations.

Mean and standard deviation of 3 evaluation metrics for registrations using 4 image pyramids. (a) registration using the Gaussian pyramid, (b) registration using the bilateral pyramid, (c) registration using the guided pyramid where the original image is the guidance image, (d) registration using the guided pyramid where the fractional differential enhanced image is the guidance image.

RMDE	7.18±7.99	6.89±7.64	6.93±7.72	6.95±7.61
RMIE	9.81±9.97	9.8±9.84	9.67±9.7	9.84±9.82
RNJD	0.67±1.82	0.59±1.73	0.58±1.72	0.56±1.63
	(a)	(b)	(c)	(d)

Experimental results demonstrate that registration using the gradient enhanced image pyramids produce improved performance over registration using the Gaussian pyramid.

Acknowledgments

The authors acknowledge the National Cancer Institute and the Foundation for the National Institutes of Health, and their critical role in the creation of the free publicly available LIDC/IDRI Database used in this study.

References

- [1] Lester, H. and Arridge, S. R., A survey of hierarchical non-linear medical image registration, *Pattern recognition*, 1, 129–149 (1999).
- [2] Hellier, P., Barillot, C., Mémin, É., and Pérez, P., Hierarchical estimation of a dense deformation field for 3-D robust registration, *IEEE Transactions on Medical Imaging*, 5, 388–402 (2001).
- [3] Christensen, G. E., Rabbitt, R. D., and Miller, M. I., 3d brain mapping using a deformable neuroanatomy, *Physics in medicine and biology*, 3, 609 (1994).
- [4] Tomasi, C. and Manduchi, R., Bilateral filtering for gray and color images, *Proc. Int. Conf. Computer Vision*, 839–846, (1998).
- [5] Zhang, M. and Gunturk, B. K., Multiresolution bilateral filtering for image denoising, *IEEE Transactions on Image Processing*, 12, 2324–2333 (2008).
- [6] Hu, Q., He, X., and Zhou, J., Multi-scale edge detection with bilateral filtering in spiral architecture, *Proc. of the Pan-Sydney area workshop on Visual information*, 29–32, (2004).
- [7] Zhang, B. and Allebach, J. P., Adaptive bilateral filter for sharpness enhancement and noise removal, *IEEE Transactions on Image Processing*, 5, 664–678 (2008).
- [8] Buades, A., Coll, B., and Morel, J.-M., The staircasing effect in neighborhood filters and its solution, *IEEE Transactions on Image Processing*, 6, 1499–1505 (2006).
- [9] He, K., Sun, J., and Tang, X., Guided image filtering, *IEEE Transactions on Pattern Analysis and Machine Intelligence*, 6, 1397–1409 (2013).
- [10] He, K., Sun, J., and Tang, X., Guided image filtering, *Computer Vision–ECCV 2010*, 1–14, (2010).
- [11] Mathieu, B., Melchior, P., Oustaloup, A., and Ceyral, C., Fractional differentiation for edge detection, *Signal Processing*, 83, 2421–2432 (2003).
- [12] Pu, Y., Wang, W., Zhou, J., Wang, Y., and Jia, H., Fractional differential approach to detecting textural features of digital image and its fractional differential filter implementation, *Science in China Series F: Information Sciences*, 51, 1319–1339 (2008).

- [13] Sparavigna, A. C. and Milligan, P., Using fractional differentiation in astronomy, *arXiv preprint arXiv:0910.4243*, (2009).
- [14] Ashburner, J. and Friston, K. J., Nonlinear spatial normalization using basis functions, *Human Brain Mapping*, 4, 254–266 (1999).
- [15] Bookstein, F., Principal warps: thin-plate splines and the decomposition of deformations, *IEEE Transactions on Pattern Analysis and Machine Intelligence*, 6, 567–585 (1989).
- [16] Biomedical Image Analysis Group, IXI dataset, (2010).
- [17] Armato, S. G. et al., The Lung Image Database Consortium (LIDC) and Image Database Resource Initiative (IDRI): a completed reference database of lung nodules on CT scans, *Med Phys*, 2, 915–931 (2011).

Author Biography

Lin Gan has a B.Sc. degree from Northwestern Polytechnical University, China, a M.Sc. degree from the University of Bristol, UK, and is currently completing his Ph.D degree with the Illinois Institute of Technology. His work has focused on image registration techniques and medical imaging.

Gady Agam is an Associate Professor of Computer Science at the Illinois Institute of Technology. His research interests include medical imaging, document imaging, machine learning, and geometric modeling.

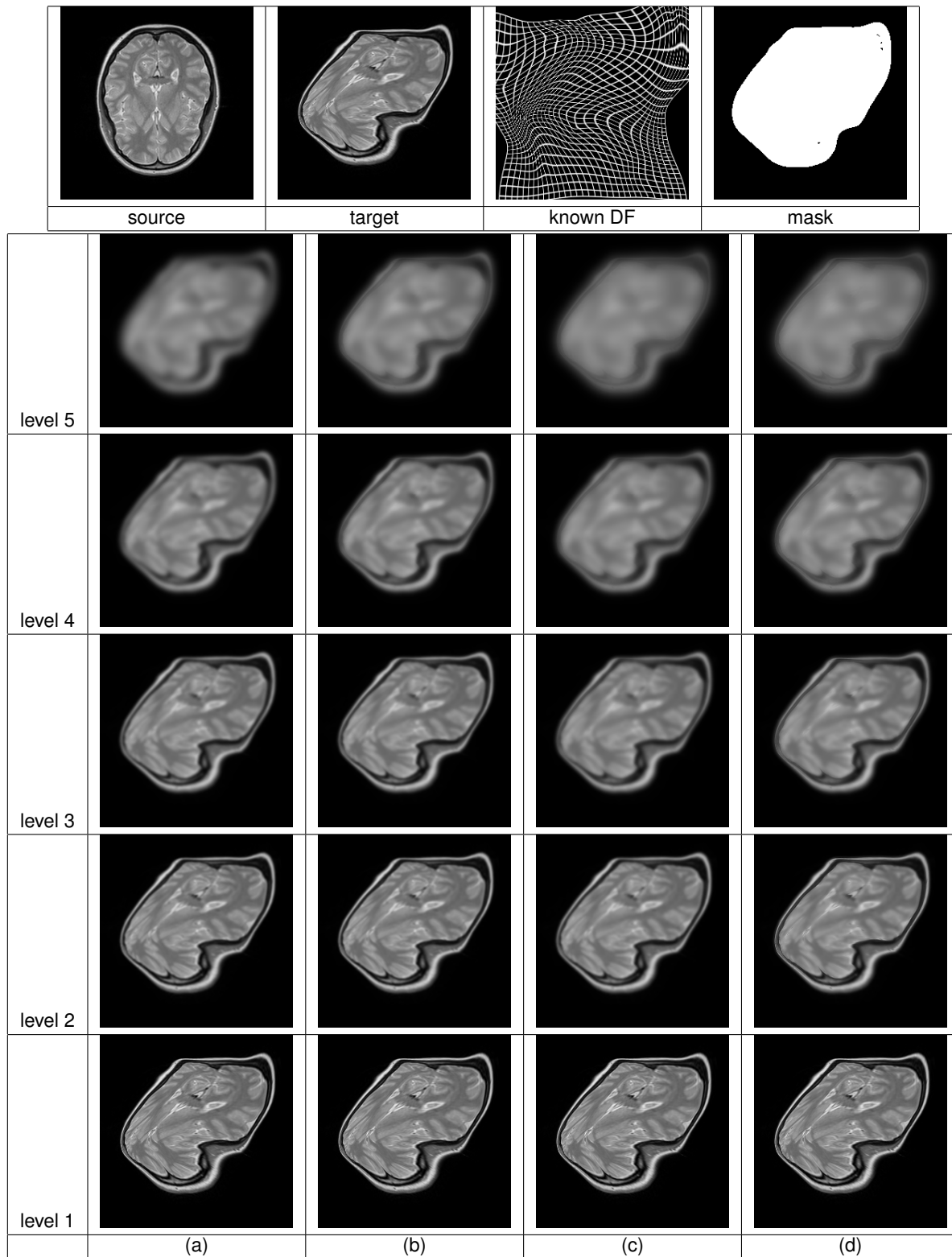


Figure 3. Image pyramids of the target image in a synthetic deformation case using 4 different image pyramids. (a) the Gaussian pyramid, (b) registration using the bilateral pyramid, (c) the guided pyramid where the original image is the guidance image, (d) the guided pyramid where the fractional differential enhanced image is the guidance image.

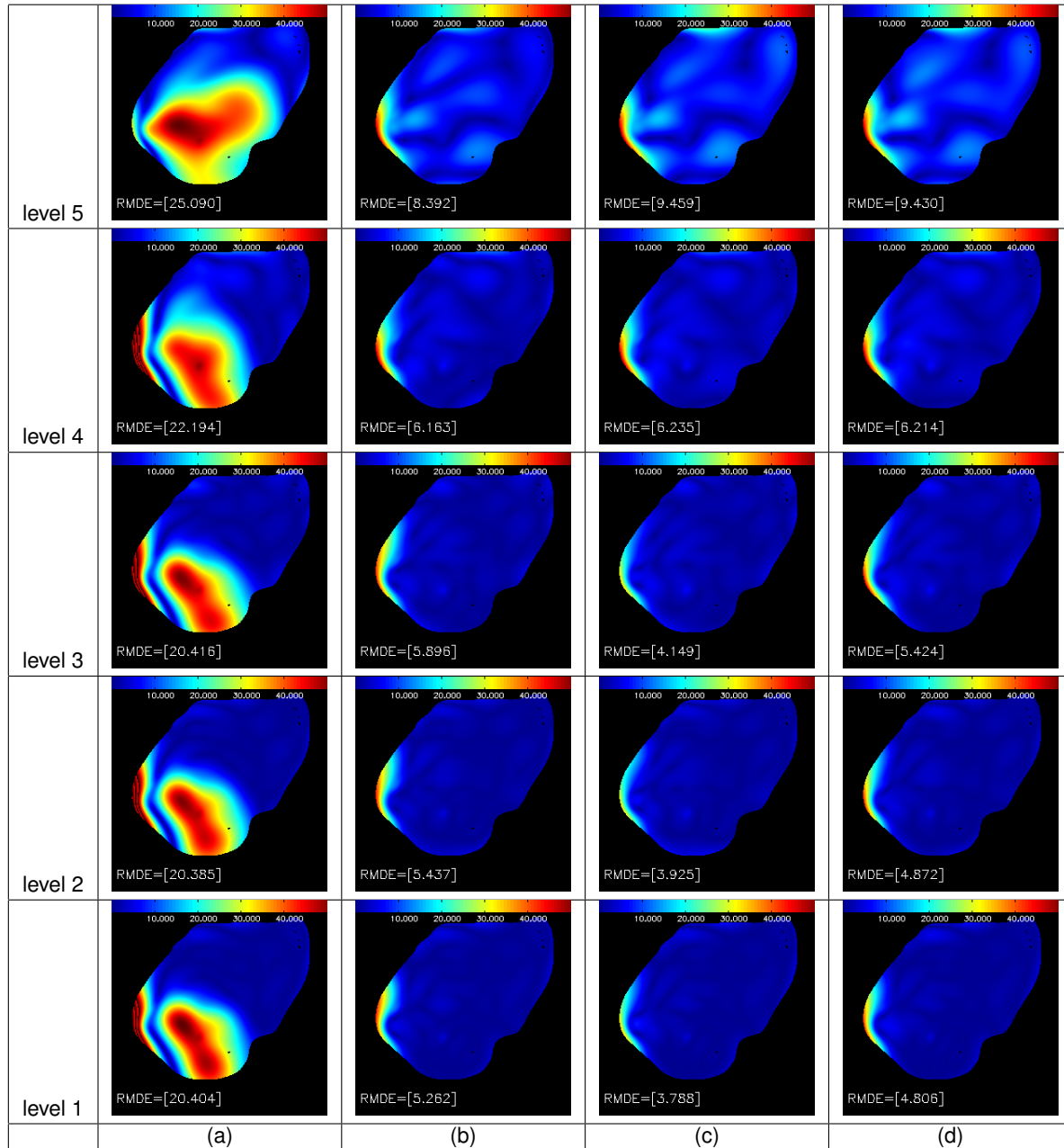


Figure 4. Deformation field error (encoded by RGB color) at each pyramid level of registrations using 4 different image pyramids on a random synthetic deformation case. (a) registration using the Gaussian pyramid, (b) registration using the bilateral pyramid, (c) registration using the guided pyramid where the original image is the guidance image, (d) registration using the guided pyramid where the fractional differential enhanced image is the guidance image.